

# DCL: Differential Contrastive Learning for Geometry-Aware Depth Synthesis

Yanchao Yang<sup>\*†</sup>  
Stanford University

Yuefan Shen<sup>\*</sup>  
Zhejiang University

Youyi Zheng<sup>†</sup>  
Zhejiang University

C. Karen Liu  
Stanford University

Leonidas Guibas  
Stanford University

## Abstract

We describe a method for realistic depth synthesis that learns diverse variations from the real depth scans and ensures geometric consistency for effective synthetic-to-real transfer. Unlike general image synthesis pipelines, where geometries are mostly ignored, we treat geometries carried by the depth based on their own existence. We propose differential contrastive learning that explicitly enforces the underlying geometric properties to be invariant regarding the real variations been learned. The resulting depth synthesis method is task-agnostic and can be used for training any task-specific networks with synthetic labels. We demonstrate the effectiveness of the proposed method by extensive evaluations on downstream real-world geometric reasoning tasks. We show our method achieves better synthetic-to-real transfer performance than the other state-of-the-art. When fine-tuned on a small number of real-world annotations, our method can even surpass the fully supervised baselines.

## 1. Introduction

Unpaired realistic depth synthesis is important in transferring annotations for geometric reasoning tasks from simulation, where labels can be automatically generated while label generation in the real world is expensive. For example, obtaining pixel-level surface normal annotations is much more difficult in the real world than in simulation. However, directly training networks on the clean synthetic depth maps will not yield satisfactory performance when testing on the real depth due to the covariate shift. There exist many works on realistic image synthesis based on generative adversarial networks, yet, there are only a few on realistic depth synthesis. Since depth maps can be viewed as gray-scale images, i.e., one could apply any image synthesis method on depth,

then why would one want to deal with depth synthesis differently?

The main reason for us to treat depth on its own but not as general image synthesis lies in the fact that depth maps are 2.5D representations of the scene, and the geometric properties carried in depth maps deserve their own existence. Traditional methods on realistic depth synthesis either model the real depth variations with an empirical noise model or add random noise and dropout to corrupt the synthetic depth. Thus, their capability to capture diverse real variations is quite limited. On the other hand, learning-based real depth synthesis methods add noise and missing regions to the synthetic depth maps by transformation networks usually trained in an adversarial manner. Despite the ability to reduce the distributional shift between the synthetic and real domains, the underlying geometric properties are not taken seriously and are always subject to undesired distortions, affecting the label transfer efficiency for downstream geometric reasoning tasks (see Fig. 1).

We treat geometric properties as first-class citizens. Moreover, we propose differential contrastive learning to learn the real-world depth variations to minimize the distributional shift between domains and explicitly enforce the underlying geometry to be consistent (for better transfer between domains). As illustrated in Fig. 3, the proposed differential contrastive learning first computes differences between features extracted at different spatial locations within each feature map of the depth (the synthetic one and its transformed version). The resulting differential features are then arranged into positive and negative samples following the terminology used in [9, 45]. More explicitly, two differential features computed at the same pair of spatial locations are considered as positive; otherwise, differential features computed at different pairs of spatial locations are considered as negative. Positive and negative samples are then used to compute the InfoNCE loss [43], which serves as the training loss, namely, the differential contrastive loss for learning depth synthesis.

<sup>\*</sup>These two authors contributed equally.

<sup>†</sup>Corresponding author.

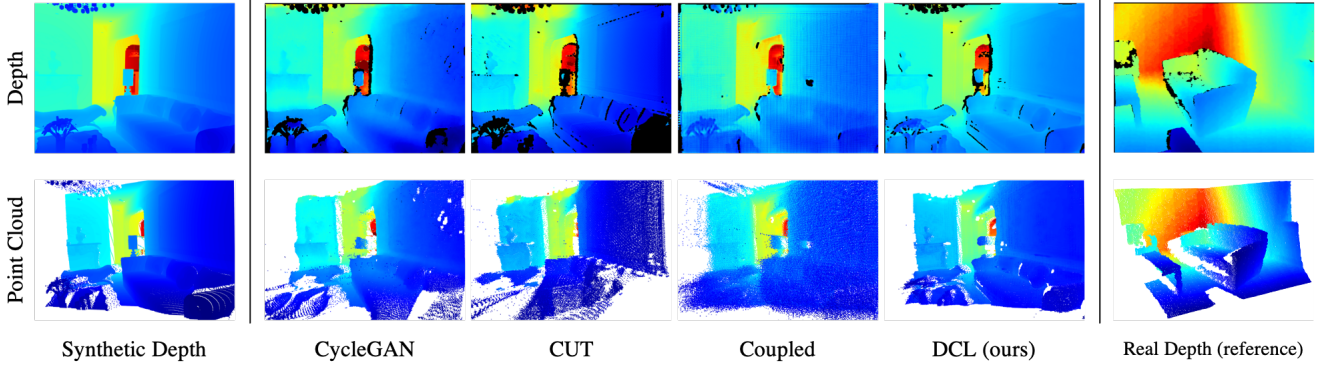


Figure 1. Synthetic to real depth synthesis. Left: clean depth map; Middle: synthesized depth map by CycleGAN [77], CUT [45], Coupled [17] and DCL (ours); Right: real depth from ScanNet [12]. Point clouds of each depth map are displayed in the second row. Note our method captures missing regions and sensor noise similar to that exhibited in the real depth map. Moreover, our method preserves the underlying geometry shown by the point cloud, i.e., ours has much fewer out-of-surface points.

The motivation of our approach drives from the observation that geometric characteristics can always be captured in the differential forms [54].<sup>1</sup> So we explicitly ask the corresponding differential features computed from the depth to be as invariant as possible against the synthesis procedure, which is then ensured by how we select positive and negative samples in the proposed differential contrastive loss. The resulting unpaired depth synthesis framework can be used for learning realistic variations from any depth sensor of any type, while preserving the geometric properties. Moreover, our approach is task agnostic, so the synthesized realistic depth maps, together with synthetic labels, can be used for training any downstream task networks in a fully supervised manner.

We perform extensive evaluations of the synthesis quality across a broad spectrum of downstream tasks, including depth enhancement, semantic segmentation, and normal estimation. The task models trained with the depth map synthesized by our method consistently achieve the best transfer performance when tested on real-world data without fine-tuning. Moreover, after fine-tuning on each task with a small portion of the labels from the real-world dataset, models pretrained with the depth maps generated by our method still outperform the models pretrained using other methods, and even surpass the supervised baselines trained with full real labels; demonstrating the proposed approach’s effectiveness in learning diverse real depth variations and preserving the underlying geometric properties of the scene.

## 2. Related Work

**Image generation and translation.** Image generation maps a random noise sampled from a prior distribution to images satisfying a predefined distribution, e.g., natural im-

ages or faces. Many works have been proposed to generate diverse and realistic images [3, 27, 40, 42, 10] based on generative adversarial networks (GAN) [15]. Please refer to [63, 44] for a detailed overview. Image translation aims to transform images from one domain to the other, e.g., style transfer, either paired [26, 50, 23] or unpaired [59, 77, 71]. Image translation can be used as a tool to reduce domain gaps, such that the labels from one domain can be used for training in the other [22, 41]. However, one should impose constraints on the translation networks to preserve task-relevant information, e.g., semantic content [38, 22, 69, 68]. Cycle-consistency has been shown effective in regularizing the translation for style transfer [77, 71, 28]. Recently, contrastive unpaired translation (CUT) [45] proposes contrastive losses on the patch-level features to explicitly enforce the similarity of the input and out images in the feature space. Moreover, [76, 5] perform synthetic-to-real translation of images such that the clean depth can be used for training single image depth estimation, and [6] utilizes GANs to generate realistic RGBD images conditioned on a single synthetic foreground object. Besides the vast development on image-to-image translation [2, 10, 30, 36, 14, 33], little effort has been devoted to depth-to-depth translation, where the translation has to align not only the domain noise but also preserve the underlying geometry that is crucial for downstream geometric inferences based on depth maps.

**Contrastive learning.** Based on the InfoNCE loss [43], contrastive learning has been shown effective for self-supervised representation learning [20, 9, 60, 16, 7, 55]. The critical ingredient of contrastive learning is the selection of variations to which we would like the learned representations to be invariant [47, 61]. Our primary task is not to learn representations that share the invariance of the downstream tasks. Instead, we learn the real domain variations and utilize contrastive learning to take care of geo-

<sup>1</sup>For example, normals can be calculated by differentiating the surface.

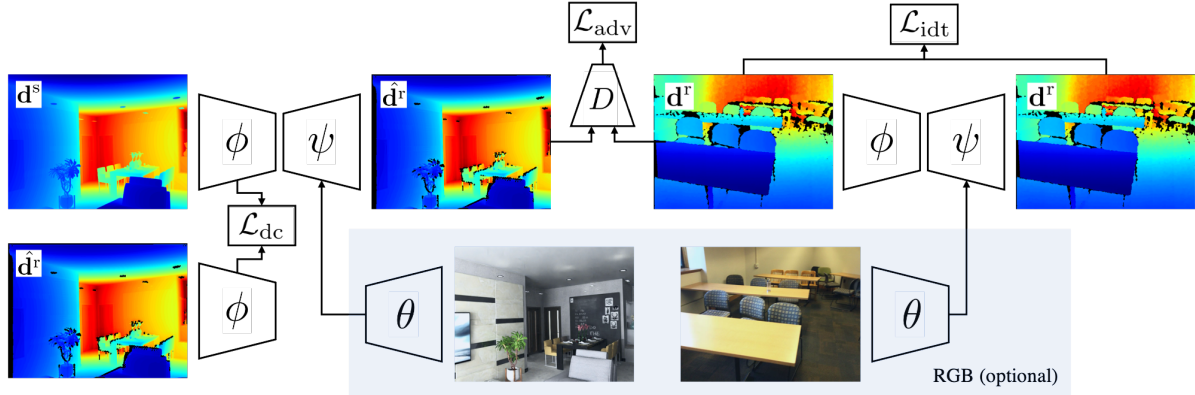


Figure 2. Overview of our method. The depth synthesis network is composed of  $\phi$  (encoder) and  $\psi$  (decoder). Note  $\psi$  can take in auxiliary information from the aligned RGB image through an image encoder  $\theta$ , which is optional. The three loss terms will be described in Sec. 3.

metric properties that should be invariant to the variations applied on the clean synthetic depth.

**Point cloud generation.** 3D point cloud generation is closely related to 2.5D depth map synthesis. A variational auto-encoder with multi-resolution tree networks is used in [13] to generate point clouds, while [1] studies various generative adversarial networks and proposes to generate point clouds by a Gaussian mixture model in the latent space of an autoencoder. And, [57] generates point clouds in an autoregressive manner. Instead of transforming random noise, [67] maps a set of 2D grid points to the target point cloud through deep grid deformation, and [66] proposes hierarchical modeling of shapes and points using continuous normalizing flows. Most of the point cloud generation methods focus on single objects. At the scene level, [72] generates synthetic point clouds via a virtual lidar in simulation, with point intensity added by a learned intensity renderer [64], and [39] replaces CAD models in a simulator with 3D static maps and 3D dynamic objects reconstructed from real-world cities. Moreover, [49] applies multi-scale domain alignment to point clouds of single objects and [75, 70] investigate domain adaptation on lidar point clouds for segmentation.

**Depth synthesis.** To inject realistic noise into synthetic depth maps, [29] proposes an empirical noise model of the depth sensor’s transmitter/receiver system, which captures sensor-specific noise and may not generalize to different ones. Similarly, [46] explicitly models sensor noise, material properties, and surface geometry for depth synthesis, but is limited to single CAD models. One can also add random Gaussian noise and dropout to synthesize additive sensor noise and missing regions [51, 34, 24]. Furthermore, [52] applies adversarial training to synthesize realistic hand pose images, and [4] synthesizes holes with a network trained to predict missing regions from RGB images. Similarly, [17] learns the hole prediction from real RGBD images, but relies on image translation to bring synthetic

images to the real domain such that the learned hole prediction model can be applied on synthetic RGB images. One can also apply domain adaptation for depth-based predictive tasks [35, 64]. However, these methods do not focus on generating realistic depth maps. Our method focuses on realistic depth synthesis, and the synthesized depth maps can be used for any tasks that take depth as input, so it can be used in conjunction with domain adaptation methods when the task is known. Also related are works on depth enhancement, semantic segmentation, and surface normal estimation [18, 11, 19, 62, 74, 58, 53, 37, 25, 56, 65, 48, 31, 73]. However, we treat realistic depth synthesis as our primary task and evaluate the quality of the synthesized depth maps on these tasks in a synthetic-to-real setting.

### 3. Method

Let  $\mathbf{d} \in \mathbb{R}^{H \times W}$  be a depth map, and  $\mathbf{I} \in \mathbb{R}^{H \times W \times 3}$  be the corresponding color image. Suppose we have a synthetic (clean) dataset  $\mathcal{D}^s = \{(\mathbf{d}^s, \mathbf{I}^s)\}$  and a real-world (noisy) dataset  $\mathcal{D}^r = \{(\mathbf{d}^r, \mathbf{I}^r)\}$ . Both of them contain pairs of aligned depth maps and color images. However, there is no pairing between  $\mathcal{D}^s$  and  $\mathcal{D}^r$ , a typical setting of unpaired image synthesis or translation. Our goal is to learn a mapping between the synthetic depth map  $\mathbf{d}^s$  and the real depth map  $\mathbf{d}^r$ , using only unpaired datasets  $\mathcal{D}^s$  and  $\mathcal{D}^r$ . The overall architecture of our method is illustrated in Fig. 2. Note the aligned color images are auxiliary, without which our method still runs, and we elaborate in the following.

#### 3.1. Depth-to-depth Synthesis

We first illustrate our method using only depth maps for simplicity. We then detail how color images can be incorporated as auxiliary signals to facilitate the synthesis procedure. Let  $\phi$  be an encoder, and  $\psi$  be a decoder, together they constitute the transformation network to be trained:

$$\hat{\mathbf{d}}^r = \psi(\phi(\mathbf{d}^s)) \quad (1)$$

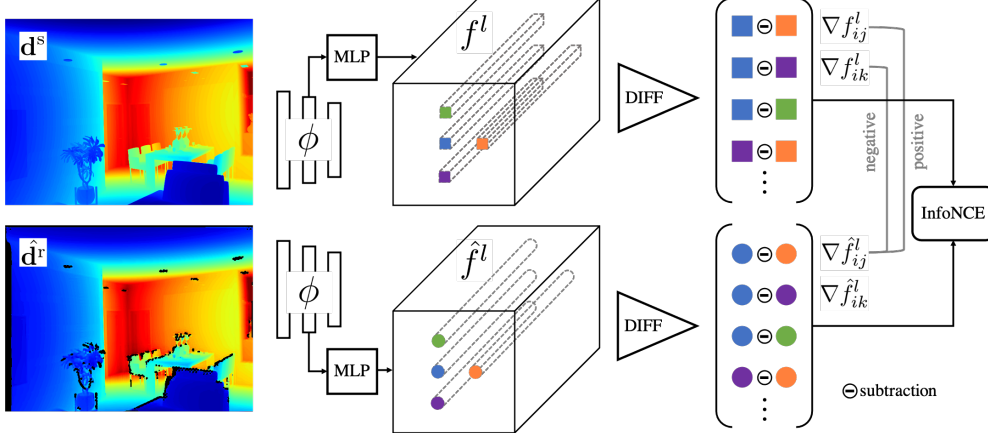


Figure 3. Differential Contrastive Learning. Given a synthetic depth map  $\mathbf{d}^s$  and the transformed noisy depth map  $\hat{\mathbf{d}}^r$ , feature maps  $f^l$  and  $\hat{f}^l$  are extracted from the  $l$ -th layer of the encoder  $\phi$ . Differential features are then computed and arranged into positive and negative samples depending on their pairwise spatial locations, e.g., differential features with the same row number are positive samples.

with  $\hat{\mathbf{d}}^r$  be the synthesized (noisy) depth map conditioned on the clean depth map  $\mathbf{d}^s$ . To enforce statistical similarity between the synthesized depth map  $\hat{\mathbf{d}}^r$  and the real depth map  $\mathbf{d}^r$ , we can apply a discriminator network  $D$  to minimize the domain discrepancy by adversarial training:

$$\mathcal{L}_{\text{adv}} = \mathbb{E}_{\mathbf{d}^r \sim \mathcal{D}^r} \log D(\mathbf{d}^r) + \mathbb{E}_{\mathbf{d}^s \sim \mathcal{D}^s} \log(1 - D(\hat{\mathbf{d}}^r)) \quad (2)$$

Since Eq. (2) only helps to reduce the distributional shift, but does not guarantee the consistency of the generated content [59, 52], CycleGAN [77] resorts to cycle consistency to constrain the transformation. On the other hand, contrastive unpaired translation (CUT) [45] eliminates the cycle consistency by applying contrastive loss on features from multiple layers of the encoder to preserve the image content. Even though it works for image-to-image translation, we observe heavy distortions on the underlying geometric structures of the synthesized depth maps, which hinder the transfer from synthetic domains to real domains.

### 3.2. Differential Contrastive Learning

We aim for a transformation  $\psi \circ \phi$  that can capture the complex noise phenomenon in real depth, and, at the same time, preserve the underlying geometry of the clean depth maps for better transfer on geometric reasoning tasks.

Since we ask for geometric invariants of the synthetic depth maps, we choose to work with the InfoNCE loss [43] due to its effectiveness in capturing invariants for self-supervised representation learning [9, 20]. However, the type of invariants that will be learned with the InfoNCE loss depends mainly on the mechanism to choose positive and negative samples. For example, in [9], an image and its color distorted version are considered as a pair of positive samples, whereas this same image and another different image are considered as negative samples. With this sam-

pling strategy, the features learned will be invariant to color distortions but still be discriminative for image identities.

Inspired by the fact that geometric properties can always be captured by their differential forms [54], we propose to impose an explicit constraint on the underlying geometry of the scene through differential contrastive learning shown in Fig. 3. Let  $f^l = \phi^l(\mathbf{d}^s)$ ,  $\hat{f}^l = \phi^l(\hat{\mathbf{d}}^r)$  be the feature maps extracted from the  $l$ -th layer of the encoder  $\phi$  applied on the synthetic depth map  $\mathbf{d}^s$  and the synthesized depth map  $\hat{\mathbf{d}}^r$ . Also, let  $f_i^l$  be the feature vector from  $f^l$  at the spatial location  $i$ . We apply the following sampling mechanism to collect positive and negative pairs:

$$\text{positive} : (\nabla \hat{f}_{ij}^l = \hat{f}_i^l - \hat{f}_j^l, \nabla f_{ij}^l = f_i^l - f_j^l) \quad (3)$$

$$\text{negative} : (\nabla \hat{f}_{ij}^l = \hat{f}_i^l - \hat{f}_k^l, \nabla f_{ik}^l = f_i^l - f_k^l) \quad (4)$$

where  $i, j, k$  are different spatial locations on the feature maps. Note each sample consists of two differential vectors (synthetic and synthesized) computed either at the same pair-wise locations (positive) or different pair-wise locations (negative) (see Fig. 3). Given the InfoNCE loss:

$$\begin{aligned} \mathcal{L}_{\text{nce}}(\nabla \hat{f}_{ij}^l, \nabla f_{ij}^l, \{\nabla f_{ik}^l\}_{k \neq j}) = \\ - \log \frac{\exp(\nabla \hat{f}_{ij}^l \cdot \nabla f_{ij}^l / \tau)}{\exp(\nabla \hat{f}_{ij}^l \cdot \nabla f_{ij}^l / \tau) + \sum_k \exp(\nabla \hat{f}_{ij}^l \cdot \nabla f_{ik}^l / \tau)} \end{aligned}$$

Our differential contrastive loss is defined as:

$$\mathcal{L}_{\text{dc}} = \mathbb{E}_{\mathbf{d}^s \sim \mathcal{D}^s} \sum_l \sum_{i,j} \mathcal{L}_{\text{nce}}(\nabla \hat{f}_{ij}^l, \nabla f_{ij}^l, \{\nabla f_{ik}^l\}_{k \neq j}) \quad (5)$$

here  $(i, j, k)$ 's can be randomly sampled to avoid enumerating the entire grid. The key insight is that, we want the differentials to be similar (invariant) before and after the transformation, i.e., the depth values may be altered due to

the noise or missing regions learned from real depth maps; however, the underlying geometric structures captured by the differentials should be similar. In other words, the proposed differential contrastive loss explicitly enforces the consistency between geometric structures of the synthetic and synthesized depth maps, while leaving enough flexibility for the transformation network to learn real variations. Note, differential contrastive losses over feature maps from multiple layers of the encoder  $\phi$  are also computed, making it possible to capture both local and global geometric properties.

Given that a global shift in the depth values might be differentiated away and thus can not be detected with the proposed differential contrastive loss<sup>2</sup>, we apply an identity loss on the real depth map  $\mathbf{d}^r$  to prevent potential global shifts in the range of the synthesized depth:

$$\mathcal{L}_{\text{idt}} = \mathbb{E}_{\mathbf{d}^r \sim \mathcal{D}^r} \|\psi(\phi(\mathbf{d}^r)) - \mathbf{d}^r\|_1 \quad (6)$$

which is the  $L1$  loss between a real depth map and its transformed version. The **final training loss** of the proposed differential contrastive learning for synthesizing realistic depth maps from synthetic ones is:

$$\mathcal{L} = \mathcal{L}_{\text{adv}} + \alpha \mathcal{L}_{\text{dc}} + \beta \mathcal{L}_{\text{idt}} \quad (7)$$

### 3.3. Incorporating RGB Images

Our method can work with only depth, yet, it may miss capturing some noise phenomenon related to the property of the surface material, e.g., reflective or even transparent surfaces, due to the lack of such information in the depth maps. To enable such capability, we can *optionally* incorporate RGB images in our depth synthesis pipeline. Specifically, we use the RGB image as an auxiliary channel for the depth decoder to exploit the surface material information.

As shown in Fig. 2, we instantiate another encoder  $\theta$ , which shares the structure of  $\phi$ . The extracted RGB image features are forwarded to the depth decoder  $\psi$  and concatenated with the depth features accordingly. Note, now we have  $\hat{\mathbf{d}}^r = \psi(\phi(\mathbf{d}^s), \theta(\mathbf{I}^s))$  instead of Eq. (1), and the training loss remains the same. We illustrate the potential usefulness of RGB images through ablations.

## 4. Experiments

We evaluate the proposed depth synthesis method on multiple downstream tasks, including depth enhancement, semantic segmentation, and normal estimation. Our goal is to have a comprehensive understanding of the capability of our method to learn the noise exhibited in the real depth (depth enhancement) while being able to transfer for both high-level (semantic segmentation) and low-level (surface normal) geometric reasonings.

<sup>2</sup>Also, there is no incentive for the discriminator to stop global shifts

Method	RMSE $\downarrow$	RMSE <sub>log</sub> $\downarrow$	MAE $\downarrow$	PSNR $\uparrow$	SSIM $\uparrow$
Baseline	0.1871	0.2871	0.0716	33.670	0.7822
Simulation [18]	0.1618	0.2819	0.0817	36.561	0.7955
CycleGAN [77]	0.1448	0.2680	0.0911	38.771	0.8469
CUT [45]	0.1757	0.4207	0.1186	34.870	0.8066
Coupled [17]	0.1273	0.2014	0.0568	41.522	0.8524
DCL w/o rgb	0.1233	0.2171	<b>0.0564</b>	42.340	0.8692
<b>DCL</b>	<b>0.1198</b>	<b>0.1871</b>	0.0650	<b>42.980</b>	<b>0.8754</b>
Supervised	0.1062	0.1123	0.0437	45.426	0.9079

Table 1. Depth enhancement without fine-tuning. Scores are computed with the networks trained using only the synthesized (noisy) depth maps and the corresponding clean depth maps. Top-performing ones are marked as bold. We report the performance of our method with and without aligned RGB images.

Method	RMSE $\downarrow$	RMSE <sub>log</sub> $\downarrow$	MAE $\downarrow$	PSNR $\uparrow$	SSIM $\uparrow$
Simulation [18]	0.1230	0.1632	0.0646	42.243	0.8498
CycleGAN [77]	0.1019	0.1114	0.0420	46.207	0.9089
CUT [45]	0.1066	0.1444	0.0440	45.231	0.8961
Coupled [17]	0.1039	0.1184	0.0405	45.882	0.9093
DCL w/o rgb	0.1041	<b>0.1023</b>	0.0417	45.882	0.9078
<b>DCL</b>	<b>0.1017</b>	0.1028	<b>0.0392</b>	<b>46.338</b>	<b>0.9140</b>
Supervised	0.1062	0.1123	0.0437	45.426	0.9079

Table 2. Depth enhancement with fine-tuning on 10% of the labels from the real domain. The top-performing ones are marked as bold. Note all methods improve after fine-tuning, and DCL consistently outperforms the supervised baseline.

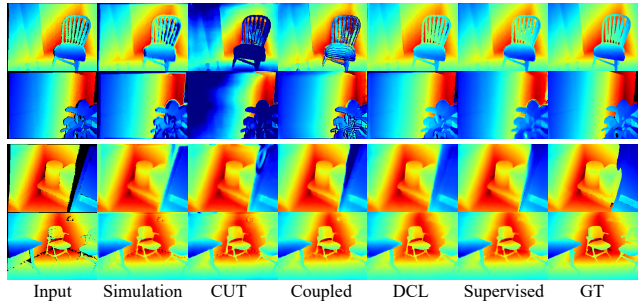


Figure 4. Visual comparison of depth enhancement. From left to right: input real depth scan, Simulation [18], CUT [45], Coupled [17], DCL(ours), supervised baseline and the ground-truth. The top two rows are results without fine-tuning, and the bottom two rows are fine-tuned with 10% of the real labels.

After training the depth synthesis, we transform the synthetic depth maps to synthesized (noisy) ones in a task agnostic manner. We then perform evaluations on each downstream task in two stages: 1) train a task-specific network using only the labels from the synthetic domain, and test the network directly on a validation set from the real domain; 2) fine-tune the previously trained task-specific networks using a small portion of the annotations from the real domain, and then test on the same real validation set as in

1). In stage one, we like to check how the synthesized depth maps mimic the real ones. In the second stage, we check the transferability of the pre-trained weights in terms of reducing the number of real annotations.

## 4.1. Training Depth Synthesis

**Datasets.** We use InteriorNet [32] as the source of synthetic data, and ScanNet [12] as the source of realistic data. The InteriorNet provides depth maps with size 640x480 rendered from 1.7M interior layouts for different scenes created by professional designers. We randomly sample 30K depth maps from InteriorNet to form the synthetic dataset. We further split them into a subset of 24K depth maps for training depth synthesis (synthesis training set), and 6K depth maps for training task-specific networks (task training set). Each sample in the synthetic dataset consists of a clean depth map, an aligned color image, and the corresponding normal and semantic segmentation mask. Similarly, we randomly sample 24K real scans from ScanNet, which contains real-world depth maps with size 640x480 collected from 1.5K indoor scenes. Each of the raw scans also comes with an aligned color image, and they are manually annotated. The ground-truth depth and normal are computed through the reconstructed meshes from multiple scans. Note the training of depth synthesis only involves the depth maps but not the task-related annotations.

**Baselines.** A natural depth synthesis baseline is the identity mapping, i.e., the clean depth with no adaptation (Baseline). We also compare with the commonly used empirical noise model [18] (Simulation), and two state-of-the-art image translation methods [77] (CycleGAN) and [45] (CUT). Moreover, we compare to [17] (Coupled), which is the current state-of-the-art on synthetic to real depth synthesis that separately models missing regions and sensor noise based on both depth and color images.

**Training details.** Our network architecture follows that of CUT [45], which employs an image transformation network consisting of ResNet blocks [21]. We extract multi-layer features from five evenly distributed layers of the encoder to compute the differential contrastive loss. Like CUT, we apply a two-layer MLP with 128 output units and  $L2$  normalization on the extracted features before passing them to the loss function. As mentioned, our method can optionally work with aligned color images. So we train our model under two different settings: one with color images encoded and concatenated with the features of the depth map (DCL); the other with only depth maps (DCL w/o rgb). We report scores for both to check if there exists improvement by incorporating extra information from the color images. For all the other methods, aligned color images are always available to the transformation network, except the empirical noise model proposed in [18], which relies only

on geometry to synthesize noise<sup>3</sup>.

All of our experiments are conducted on a server with four GeForce RTX 2080Ti GPUs, and our networks are implemented within the PyTorch framework. For the training of depth synthesis with differential contrastive loss, we use an Adam optimizer ( $\beta_1 = 0.5$  and  $\beta_2 = 0.999$ ) with an initial learning rate of 0.0002. We set the batch size to 16 and train up to 50 epochs, which can be finished within 20 hours. The weights in Eq. (7) are  $\alpha = 1.5$ ,  $\beta = 1.0$  for all quantitative comparisons, i.e., the synthesis networks for all the downstream tasks are the same one.

Now we describe the two-stage evaluations for each downstream task and report the qualitative and quantitative results. The ablation study on each loss term in Eq. (7) is reported in the appendix.

## 4.2. Depth Enhancement

After training the depth synthesis network, we convert the 6K synthetic depth maps (task training set) to realistic (noisy) ones. We train a depth enhancement network [25] for each of the synthesized noisy datasets from different synthesis methods. We also apply the depth enhancement training loss proposed in [25] for all models, which are trained using an Adam optimizer with an initial learning rate of 0.0002,  $\beta_1 = 0.5$  and  $\beta_2 = 0.999$ . The batch size is 20, and the training runs for 50 epochs (in total 3.5 hours).

When the training converges, we test each enhancement network on a preserved real validation set consists of 300 raw scans and the corresponding clean scans generated from reconstructed meshes. We report the scores under multiple evaluation metrics: root mean square error (RMSE) and its log version, mean absolute error (MAE), peak signal-to-noise ratio (PSNR), and structural similarity index measure (SSIM) following [17]. The first three measure the accuracy of the enhanced depth maps, and the latter two measure the structural similarity of the enhanced depth maps compared to the ground-truth.

As shown in Tab. 1, our method consistently achieves smaller error and higher structural similarity compared to other methods. As expected, the empirical noise model (Simulation) [18] generally performs worse than the learning-based methods. Note that CUT [45] performs even worse than Simulation<sup>4</sup>. We conjecture that CUT may capture biased real noise. Hence, its performance is not even as good as the empirical noise model that randomly adds noise without looking at the real scans. We also include the score from a purely supervised model that is trained on a separate training set of 3000 real depth scans to provide a reference on the desired real domain performance<sup>5</sup>.

<sup>3</sup>For example, surface normal is used to synthesize missing regions.

<sup>4</sup>We have tuned CUT and other competing methods using grid search for their optimal hyper-parameters.

<sup>5</sup>This training set is different from both the real validation set and the

Method	wall	floor	cabinet	bed	chair	sofa	table	door	window	desk	curtain	ceiling	fridge	tv	others	mIoU-15	mIoU-12	mIoU-9
Baseline	39.52	41.90	2.96	0.97	0.04	5.45	1.97	1.25	2.50	0.0	2.90	4.75	0.0	0.0	9.78	7.60	9.50	12.33
Simulation [18]	38.50	47.67	10.47	<b>22.40</b>	<b>8.88</b>	10.30	9.49	2.31	4.77	3.05	3.97	28.72	0.03	0.0	13.63	13.61	16.27	17.82
CycleGAN [77]	39.11	47.47	10.39	21.48	6.49	9.14	<b>9.99</b>	1.56	4.22	2.47	4.37	<b>30.12</b>	0.04	0.0	14.31	13.41	16.22	17.85
CUT [45]	45.23	60.49	<b>12.84</b>	13.03	4.34	9.37	5.72	4.55	6.76	1.66	8.43	22.46	0.83	0.84	11.98	13.90	16.88	20.23
Coupled [17]	38.85	25.47	8.52	13.57	3.33	2.28	1.02	4.44	2.99	0.84	8.56	21.11	0.14	0.09	11.15	9.49	11.57	13.71
DCL w/o rgb	45.05	55.23	12.81	19.35	5.50	10.17	7.22	<b>7.41</b>	<b>7.77</b>	<b>3.75</b>	7.79	23.03	0.09	<b>2.65</b>	12.32	14.73	<b>17.66</b>	20.17
DCL	<b>46.11</b>	<b>67.53</b>	10.48	10.04	8.16	<b>11.65</b>	4.52	3.16	4.68	2.81	<b>8.72</b>	26.67	<b>1.06</b>	0.13	<b>15.30</b>	<b>14.74</b>	17.64	<b>21.59</b>
Supervised	72.43	88.45	52.57	70.97	54.15	55.60	52.83	36.30	34.31	43.25	37.66	81.64	22.65	56.18	39.25	53.22	55.44	55.36

Table 3. Semantic segmentation without fine-tuning. We report the intersection-over-union (IoU) scores for each class, and the mean intersection-over-union (mIoU) scores over a subset of semantic classes (mIoU-15, mIoU-12, mIoU-9). DCL performs well for most of the classes and consistently outperforms the other methods in terms of mIoUs.

Method	wall	floor	cabinet	bed	chair	sofa	table	door	window	desk	curtain	ceiling	fridge	tv	others	mIoU-15	mIoU-12	mIoU-9
Baseline	62.10	74.24	29.17	48.44	39.35	41.83	19.54	21.75	31.97	27.78	29.49	70.11	6.62	25.19	28.30	37.06	40.39	43.22
Simulation [18]	72.58	85.91	42.49	63.88	53.90	59.04	55.92	37.72	47.06	33.50	41.91	79.18	17.47	<b>45.27</b>	36.27	51.47	54.62	55.80
CycleGAN [77]	71.50	86.24	44.29	63.32	53.43	53.75	53.96	37.56	43.96	35.81	42.46	76.09	19.60	40.95	36.51	50.63	53.79	54.71
CUT [45]	70.80	86.95	40.47	58.69	53.60	46.04	53.37	34.82	46.22	33.72	47.53	83.52	17.65	40.97	34.81	49.94	53.08	54.57
Coupled [17]	71.82	86.54	42.55	64.03	54.12	53.91	55.25	33.05	42.85	32.82	42.40	78.21	14.81	38.43	35.35	49.74	53.23	54.08
DCL w/o rgb	<b>75.62</b>	<b>87.56</b>	49.50	<b>69.84</b>	58.01	59.81	60.91	<b>43.22</b>	51.78	<b>42.09</b>	<b>47.90</b>	<b>83.53</b>	<b>38.51</b>	44.75	42.15	<b>57.01</b>	59.49	<b>60.12</b>
DCL	75.61	87.48	<b>49.77</b>	69.82	<b>58.36</b>	<b>59.95</b>	<b>61.11</b>	42.95	<b>51.92</b>	42.05	47.70	83.20	38.04	44.64	<b>42.27</b>	56.99	<b>59.49</b>	60.10
Supervised	72.43	88.45	52.57	70.97	54.15	55.60	52.83	36.30	34.31	43.25	37.66	81.64	22.65	56.18	39.25	53.22	55.44	55.36

Table 4. Semantic segmentation with fine-tuning on 25% of the annotations from the real domain. All methods improve, especially, the fine-tuned models outperform the supervised baseline by a large margin on classes that appear more frequently in the synthetic environment, e.g., window and curtain. DCL gains the most from the fine-tuning and outperforms the supervised one by an overall margin of 7.2%.

We also fine-tune the models trained with the synthesized depth using 10% of the annotations from the real training set that is used to train the supervised baseline in Tab. 1. Moreover, we report the scores after supervised fine-tuning in Tab. 2. Interestingly, the fine-tuned model with CUT now performs better than the empirical noise model (Simulation). As observed, our model surpasses the supervised baseline on all metrics, which confirms that the parameters learned using our synthesized depth maps can transfer to the real domain on depth enhancement and transfer better than the competing depth synthesis methods. Please see Fig. 4 for visual comparisons.

### 4.3. Semantic Segmentation

We use the synthesized depth maps and their ground-truth semantic segmentation masks to train DeepLabv3+ [8] for semantic segmentation. We apply the cross-entropy loss with an initial learning rate of 0.0002, an Adam optimizer ( $\beta_1 = 0.5$  and  $\beta_2 = 0.999$ ), and a batch size of 24 for 50 epochs. Due to the class imbalance between InteriorNet and ScanNet (see appendix), we choose a set of fifteen classes for training since our goal is to validate the synthesis net-

one that is used for training depth synthesis models.

Method	Median ↓	Mean ↓	11.25 ↑	16 ↑	22.5 ↑	30 ↑
Baseline	21.127	24.907	0.278	0.392	0.541	0.679
Simulation [18]	23.725	27.473	0.252	0.349	0.485	0.623
CycleGAN [77]	22.321	25.454	0.283	0.367	0.501	0.653
CUT [45]	22.492	25.082	0.263	0.361	0.507	0.665
Coupled [17]	20.049	24.629	0.311	0.420	0.557	0.677
DCL w/o rgb	19.793	24.515	0.323	0.432	0.563	0.673
DCL	<b>18.920</b>	<b>23.805</b>	<b>0.334</b>	<b>0.444</b>	<b>0.579</b>	<b>0.693</b>
Supervised	8.950	14.420	0.593	0.725	0.814	0.868

Table 5. Normal estimation on real depth scans. Networks are trained with synthesized depth and corresponding normal maps.

works' performance for learning realistic sensor noise but not to adapt for class imbalance. After training, we test the semantic segmentation networks on a preserved real validation set from ScanNet. This validation set contains 600 raw depth scans and the corresponding ground-truth. We also report the performance of a purely supervised model trained with 6000 manually annotated real depth scans from ScanNet, again no overlap with the real validation set and the training set for synthesis.

We use the intersection-over-union (IoU) score to mea-

Method	Median ↓	Mean ↓	11.25 ↑	16 ↑	22.5 ↑	30 ↑
Baseline	8.955	14.900	0.588	0.710	0.798	0.854
Simulation [18]	7.806	14.017	0.630	0.731	0.807	0.859
CycleGAN [77]	10.607	16.240	0.533	0.674	0.776	0.841
CUT [45]	7.694	14.069	0.629	0.728	0.804	0.856
Coupled [17]	9.754	15.636	0.554	0.683	0.783	0.846
DCL w/o rgb	<b>7.462</b>	14.039	0.634	0.725	0.798	0.851
DCL	7.588	<b>13.810</b>	<b>0.638</b>	<b>0.738</b>	<b>0.812</b>	<b>0.862</b>
Supervised	8.950	14.420	0.593	0.725	0.814	0.868

Table 6. Normal estimation on real depth with networks trained on the synthesized depth and then fine-tuned with 10% of the annotations from the training set of the supervised baseline.

sure the quality of the predicted semantic masks. We also report the mean intersection-over-union (mIoU) scores across different subsets of classes in Tab. 3. As expected, the baseline model (Baseline) trained with only clean depth performs the worst. Moreover, the state-of-the-art depth synthesis method Coupled [17] now lags compared to other learning-based methods. Our method still achieves the best performance on most of the classes and the mean IoUs. However, due to the imbalanced class distributions, we can still observe a gap compared to the supervised baseline.

To check how the pre-trained weights help reduce the number of real-world annotations needed for semantic segmentation, we further apply fine-tuning on the pre-trained models with 25% of the annotations of the supervised baseline. We report the scores in Tab. 4. As observed, models pre-trained with our method now surpass the supervised baseline on most of the entries, and achieve the best performance compared to other competing methods. The baseline trained with clean depth is now having difficulty adapting to the real domain even after fine-tuning. Moreover, we find that all the fine-tuned models have higher scores in classes that appear more frequently in the synthetic domain, e.g., window and curtain. Interestingly, due to the bias in capturing the real-world variations, all the other learning-based methods now perform worse than simulation [18]. However, this is not true for DCL, which confirms the capability of the proposed differential contrastive learning in capturing, in an unbiased manner, the diverse real variations. Please see Fig. 5 for visual comparisons.

#### 4.4. Surface Normal Estimation

We evaluate the quality of the synthesized depth maps on normal estimation. Performance on normal estimation can measure how well the synthesized depth maps preserve the underlying geometry since the surface normal is the cross product of partial derivatives. We train the same architecture used for depth enhancement using the L1 loss between predicted normal maps and the ground-truth for 50 epochs, with an initial learning rate of 0.0002, an Adam

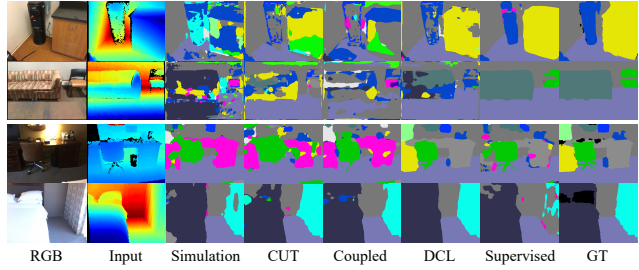


Figure 5. Visual comparison on semantic segmentation from real depth. Left to right: the aligned RGB image, input real scan, the result of Simulation [18], CUT [45], Coupled [17], DCL (ours), the supervised baseline, and the ground-truth. The top two rows are before fine-tuning, and the bottom two rows are fine-tuned.

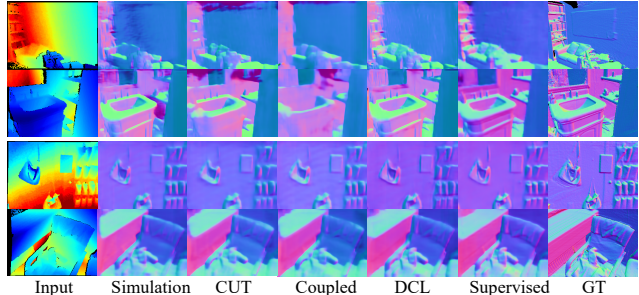


Figure 6. Visual comparison on normal estimation. Left to right: input real scan, the result of Simulation [18], CUT [45], Coupled [17], DCL(ours) and the supervised baseline. The top two rows are before fine-tuning, and the bottom two rows are fine-tuned.

optimizer( $\beta_1 = 0.5$  and  $\beta_2 = 0.999$ ), and a batch size of 20. And we report the angular errors and accuracy.

As shown in Tab. 5, the empirical noise model based method [18] (Simulation) is now significantly worse than the baseline trained with clean depth maps (Baseline), which signals that randomly adding noise may destroy the underlying geometry. The same phenomenon is also observed for two other learning-based methods (CycleGAN and CUT). Again, our method achieves the best performance on all the evaluation metrics.

Like previous tasks, we also fine-tune the pre-trained models using 10% of the real-world annotations from the training set of the supervised baseline. And we report the scores after fine-tuning in Tab. 6. All methods improve, and our method maintains the top performance thanks to the constraints on the underlying geometric properties imposed by the differential contrastive learning mechanism. Also, please refer to Fig. 6 for visual results.

## 5. Discussion

We have proposed an effective synthetic-to-real depth synthesis method based on differential contrastive learning, which enforces the differentials to be invariant to the synthesis procedure. Extensive evaluations on downstream ge-

ometric reasoning tasks indicate that our method learns diverse variations from the real scans and preserves the geometric information crucial for real-world applications. Our method is end-to-end trainable and does not need to deal with hole generation and value degeneration separately. In the future, we would like to extend our method to higher-order differentials. Moreover, since our synthesis method is task-agnostic, we like to see it be used with other task-specific domain adaptation techniques to further improve real-world performance.

## References

[1] Panos Achlioptas, Olga Diamanti, Ioannis Mitliagkas, and Leonidas Guibas. Learning representations and generative models for 3d point clouds. In *International conference on machine learning*, pages 40–49. PMLR, 2018. 3

[2] Amjad Almahairi, Sai Rajeshwar, Alessandro Sordoni, Philip Bachman, and Aaron Courville. Augmented cyclegan: Learning many-to-many mappings from unpaired data. In *International Conference on Machine Learning*, pages 195–204. PMLR, 2018. 2

[3] Martin Arjovsky, Soumith Chintala, and Léon Bottou. Wasserstein generative adversarial networks. In *International conference on machine learning*, pages 214–223. PMLR, 2017. 2

[4] Amir Atapour-Abarghouei, Samet Akcay, Gregoire Payen de La Garanderie, and Toby P Breckon. Generative adversarial framework for depth filling via wasserstein metric, cosine transform and domain transfer. *Pattern Recognition*, 91:232–244, 2019. 3

[5] Amir Atapour-Abarghouei and Toby P Breckon. Real-time monocular depth estimation using synthetic data with domain adaptation via image style transfer. In *Proceedings of the IEEE Conference on Computer Vision and Pattern Recognition*, pages 2800–2810, 2018. 2

[6] Konstantinos Bousmalis, Nathan Silberman, David Dohan, Dumitru Erhan, and Dilip Krishnan. Unsupervised pixel-level domain adaptation with generative adversarial networks. In *Proceedings of the IEEE conference on computer vision and pattern recognition*, pages 3722–3731, 2017. 2

[7] Mathilde Caron, Ishan Misra, Julien Mairal, Priya Goyal, Piotr Bojanowski, and Armand Joulin. Unsupervised learning of visual features by contrasting cluster assignments. *arXiv preprint arXiv:2006.09882*, 2020. 2

[8] Liang-Chieh Chen, Yukun Zhu, George Papandreou, Florian Schroff, and Hartwig Adam. Encoder-decoder with atrous separable convolution for semantic image segmentation. In *Proceedings of the European conference on computer vision (ECCV)*, pages 801–818, 2018. 7

[9] Ting Chen, Simon Kornblith, Mohammad Norouzi, and Geoffrey Hinton. A simple framework for contrastive learning of visual representations. In *International conference on machine learning*, pages 1597–1607. PMLR, 2020. 1, 2, 4

[10] Yunjey Choi, Minje Choi, Munyoung Kim, Jung-Woo Ha, Sunghun Kim, and Jaegul Choo. Stargan: Unified generative adversarial networks for multi-domain image-to-image translation. In *Proceedings of the IEEE conference on computer vision and pattern recognition*, pages 8789–8797, 2018. 2

[11] Camille Couprie, Clément Farabet, Laurent Najman, and Yann LeCun. Indoor semantic segmentation using depth information. *arXiv preprint arXiv:1301.3572*, 2013. 3

[12] Angela Dai, Angel X Chang, Manolis Savva, Maciej Halber, Thomas Funkhouser, and Matthias Nießner. Scannet: Richly-annotated 3d reconstructions of indoor scenes. In *Proceedings of the IEEE Conference on Computer Vision and Pattern Recognition*, pages 5828–5839, 2017. 2, 6

[13] Matheus Gadelha, Rui Wang, and Subhransu Maji. Multiresolution tree networks for 3d point cloud processing. In *Proceedings of the European Conference on Computer Vision (ECCV)*, pages 103–118, 2018. 3

[14] Aaron Gokaslan, Vivek Ramanujan, Daniel Ritchie, Kwang In Kim, and James Tompkin. Improving shape deformation in unsupervised image-to-image translation. In *Proceedings of the European Conference on Computer Vision (ECCV)*, September 2018. 2

[15] Ian J Goodfellow, Jean Pouget-Abadie, Mehdi Mirza, Bing Xu, David Warde-Farley, Sherjil Ozair, Aaron Courville, and Yoshua Bengio. Generative adversarial networks. *arXiv preprint arXiv:1406.2661*, 2014. 2

[16] Jean-Bastien Grill, Florian Strub, Florent Altché, Corentin Tallec, Pierre H Richemond, Elena Buchatskaya, Carl Doersch, Bernardo Avila Pires, Zhaohan Daniel Guo, Mohammad Gheshlaghi Azar, et al. Bootstrap your own latent: A new approach to self-supervised learning. *arXiv preprint arXiv:2006.07733*, 2020. 2

[17] Xiao Gu, Yao Guo, Fani Deligianni, and Guang-Zhong Yang. Coupled real-synthetic domain adaptation for real-world deep depth enhancement. *IEEE Transactions on Image Processing*, 29:6343–6356, 2020. 2, 3, 5, 6, 7, 8

[18] Ankur Handa, Viorica Patraucean, Vijay Badrinarayanan, Simon Stent, and Roberto Cipolla. Understanding real world indoor scenes with synthetic data. In *Proceedings of the IEEE conference on computer vision and pattern recognition*, pages 4077–4085, 2016. 3, 5, 6, 7, 8

[19] Caner Hazirbas, Lingni Ma, Csaba Domokos, and Daniel Cremers. Fusenet: Incorporating depth into semantic segmentation via fusion-based cnn architecture. In *Asian conference on computer vision*, pages 213–228. Springer, 2016. 3

[20] Kaiming He, Haoqi Fan, Yuxin Wu, Saining Xie, and Ross Girshick. Momentum contrast for unsupervised visual representation learning. In *Proceedings of the IEEE/CVF Conference on Computer Vision and Pattern Recognition*, pages 9729–9738, 2020. 2, 4

[21] Kaiming He, Xiangyu Zhang, Shaoqing Ren, and Jian Sun. Deep residual learning for image recognition. In *Proceedings of the IEEE conference on computer vision and pattern recognition*, pages 770–778, 2016. 6

[22] Judy Hoffman, Eric Tzeng, Taesung Park, Jun-Yan Zhu, Phillip Isola, Kate Saenko, Alexei Efros, and Trevor Darrell. Cycada: Cycle-consistent adversarial domain adaptation. In *International conference on machine learning*, pages 1989–1998. PMLR, 2018. 2

[23] Phillip Isola, Jun-Yan Zhu, Tinghui Zhou, and Alexei A Efros. Image-to-image translation with conditional adversarial networks. In *Proceedings of the IEEE conference on computer vision and pattern recognition*, pages 1125–1134, 2017. 2

[24] Thorbjørn Mosekjær Iversen and Dirk Kraft. Generation of synthetic kinect depth images based on empirical noise model. *Electronics Letters*, 53(13):856–858, 2017. 3

[25] Junho Jeon and Seungyong Lee. Reconstruction-based pairwise depth dataset for depth image enhancement using cnn. In *Proceedings of the European Conference on Computer Vision (ECCV)*, pages 422–438, 2018. 3, 6

[26] Levent Karacan, Zeynep Akata, Aykut Erdem, and Erkut Erdem. Learning to generate images of outdoor scenes from attributes and semantic layouts. *arXiv preprint arXiv:1612.00215*, 2016. 2

[27] Tero Karras, Timo Aila, Samuli Laine, and Jaakko Lehtinen. Progressive growing of gans for improved quality, stability, and variation. *arXiv preprint arXiv:1710.10196*, 2017. 2

[28] Taeksoo Kim, Moonsu Cha, Hyunsoo Kim, Jung Kwon Lee, and Jiwon Kim. Learning to discover cross-domain relations with generative adversarial networks. In *International Conference on Machine Learning*, pages 1857–1865. PMLR, 2017. 2

[29] Michael J Landau, Benjamin Y Choo, and Peter A Beling. Simulating kinect infrared and depth images. *IEEE transactions on cybernetics*, 46(12):3018–3031, 2015. 3

[30] Hsin-Ying Lee, Hung-Yu Tseng, Jia-Bin Huang, Maneesh Singh, and Ming-Hsuan Yang. Diverse image-to-image translation via disentangled representations. In *Proceedings of the European conference on computer vision (ECCV)*, pages 35–51, 2018. 2

[31] Bo Li, Chunhua Shen, Yuchao Dai, Anton Van Den Hengel, and Mingyi He. Depth and surface normal estimation from monocular images using regression on deep features and hierarchical crfs. In *Proceedings of the IEEE conference on computer vision and pattern recognition*, pages 1119–1127, 2015. 3

[32] Wenbin Li, Sajad Saeedi, John McCormac, Ronald Clark, Dimos Tzoumanikas, Qing Ye, Yuzhong Huang, Rui Tang, and Stefan Leutenegger. Interiornet: Mega-scale multi-sensor photo-realistic indoor scenes dataset. *arXiv preprint arXiv:1809.00716*, 2018. 6

[33] Xiaodan Liang, Hao Zhang, Liang Lin, and Eric Xing. Generative semantic manipulation with mask-contrasting gan. In *Proceedings of the European Conference on Computer Vision (ECCV)*, pages 558–573, 2018. 2

[34] Yuval Litvak, Armin Biess, and Aharon Bar-Hillel. Learning pose estimation for high-precision robotic assembly using simulated depth images. In *2019 International Conference on Robotics and Automation (ICRA)*, pages 3521–3527. IEEE, 2019. 3

[35] Keng-Chi Liu, Yi-Ting Shen, Jan P. Klopp, and Liang-Gee Chen. What synthesis is missing: Depth adaptation integrated with weak supervision for indoor scene parsing. In *Proceedings of the IEEE/CVF International Conference on Computer Vision (ICCV)*, October 2019. 3

[36] Ming-Yu Liu, Xun Huang, Arun Mallya, Tero Karras, Timo Aila, Jaakko Lehtinen, and Jan Kautz. Few-shot unsupervised image-to-image translation. In *Proceedings of the IEEE/CVF International Conference on Computer Vision*, pages 10551–10560, 2019. 2

[37] Si Lu, Xiaofeng Ren, and Feng Liu. Depth enhancement via low-rank matrix completion. In *Proceedings of the IEEE conference on computer vision and pattern recognition*, pages 3390–3397, 2014. 3

[38] Liqian Ma, Xu Jia, Stamatios Georgoulis, Tinne Tuytelaars, and Luc Van Gool. Exemplar guided unsupervised image-to-image translation with semantic consistency. *arXiv preprint arXiv:1805.11145*, 2018. 2

[39] Sivabalan Manivasagam, Shenlong Wang, Kelvin Wong, Wenyuan Zeng, Mikita Sazanovich, Shuhan Tan, Bin Yang, Wei-Chiu Ma, and Raquel Urtasun. Lidarsim: Realistic lidar simulation by leveraging the real world. In *Proceedings of the IEEE/CVF Conference on Computer Vision and Pattern Recognition*, pages 11167–11176, 2020. 3

[40] Xudong Mao, Qing Li, Haoran Xie, Raymond YK Lau, Zhen Wang, and Stephen Paul Smolley. Least squares generative adversarial networks. In *Proceedings of the IEEE international conference on computer vision*, pages 2794–2802, 2017. 2

[41] Zak Murez, Soheil Kolouri, David Kriegman, Ravi Ramamoorthi, and Kyungnam Kim. Image to image translation for domain adaptation. In *Proceedings of the IEEE Conference on Computer Vision and Pattern Recognition*, pages 4500–4509, 2018. 2

[42] Augustus Odena, Christopher Olah, and Jonathon Shlens. Conditional image synthesis with auxiliary classifier gans. In *International conference on machine learning*, pages 2642–2651. PMLR, 2017. 2

[43] Aaron van den Oord, Yazhe Li, and Oriol Vinyals. Representation learning with contrastive predictive coding. *arXiv preprint arXiv:1807.03748*, 2018. 1, 2, 4

[44] Zhaoqing Pan, Weijie Yu, Xiaokai Yi, Asifullah Khan, Feng Yuan, and Yuhui Zheng. Recent progress on generative adversarial networks (gans): A survey. *IEEE Access*, 7:36322–36333, 2019. 2

[45] Taesung Park, Alexei A. Efros, Richard Zhang, and Jun-Yan Zhu. Contrastive learning for conditional image synthesis. In *ECCV*, 2020. 1, 2, 4, 5, 6, 7, 8

[46] Benjamin Planche, Ziyuan Wu, Kai Ma, Shanhui Sun, Stefan Kluckner, Oliver Lehmann, Terrence Chen, Andreas Hutter, Sergey Zakharov, Harald Kosch, et al. Depthsynth: Real-time realistic synthetic data generation from cad models for 2.5 d recognition. In *2017 International Conference on 3D Vision (3DV)*, pages 1–10. IEEE, 2017. 3

[47] Senthil Purushwalkam and Abhinav Gupta. Demystifying contrastive self-supervised learning: Invariances, augmentations and dataset biases. *arXiv preprint arXiv:2007.13916*, 2020. 2

[48] Xiaojuan Qi, Renjie Liao, Zhengzhe Liu, Raquel Urtasun, and Jiaya Jia. Geonet: Geometric neural network for joint depth and surface normal estimation. In *Proceedings of the IEEE Conference on Computer Vision and Pattern Recognition*, pages 283–291, 2018. 3

[49] Can Qin, Haoxuan You, Lichen Wang, C-C Jay Kuo, and Yun Fu. Pointdan: A multi-scale 3d domain adaption network for point cloud representation. *Advances in Neural Information Processing Systems*, 32:7192–7203, 2019. 3

[50] Patsorn Sangkloy, Jingwan Lu, Chen Fang, Fisher Yu, and James Hays. Scribbler: Controlling deep image synthesis with sketch and color. In *Proceedings of the IEEE Conference on Computer Vision and Pattern Recognition*, pages 5400–5409, 2017. 2

[51] Lama Seoud, Jonathan Boisvert, Marc-Antoine Drouin, Michel Picard, and Guy Godin. Increasing the robustness of cnn-based human body segmentation in range images by modeling sensor-specific artifacts. In *Proceedings of the European Conference on Computer Vision (ECCV) Workshops*, pages 0–0, 2018. 3

[52] Ashish Shrivastava, Tomas Pfister, Oncel Tuzel, Joshua Susskind, Wenda Wang, and Russell Webb. Learning from simulated and unsupervised images through adversarial training. In *Proceedings of the IEEE conference on computer vision and pattern recognition*, pages 2107–2116, 2017. 3, 4

[53] Xibin Song, Yuchao Dai, Dingfu Zhou, Liu Liu, Wei Li, Hongdong Li, and Ruigang Yang. Channel attention based iterative residual learning for depth map super-resolution. In *Proceedings of the IEEE/CVF Conference on Computer Vision and Pattern Recognition*, pages 5631–5640, 2020. 3

[54] Michael D Spivak. *A comprehensive introduction to differential geometry*. Publish or perish, 1970. 2, 4

[55] Aravind Srinivas, Michael Laskin, and Pieter Abbeel. Curl: Contrastive unsupervised representations for reinforcement learning. *arXiv preprint arXiv:2004.04136*, 2020. 2

[56] Vladimiros Sterzentsenko, Leonidas Saroglou, Anargyros Chatzitofis, Spyridon Thermos, Nikolaos Zioulis, Alexandros Doumanoglou, Dimitrios Zarpalas, and Petros Daras. Self-supervised deep depth denoising. In *Proceedings of the IEEE International Conference on Computer Vision*, pages 1242–1251, 2019. 3

[57] Yongbin Sun, Yue Wang, Ziwei Liu, Joshua Siegel, and Sanjay Sarma. Pointgrow: Autoregressively learned point cloud generation with self-attention. In *Proceedings of the IEEE/CVF Winter Conference on Applications of Computer Vision*, pages 61–70, 2020. 3

[58] Chris Sweeney, Greg Izatt, and Russ Tedrake. A supervised approach to predicting noise in depth images. In *2019 International Conference on Robotics and Automation (ICRA)*, pages 796–802. IEEE, 2019. 3

[59] Yaniv Taigman, Adam Polyak, and Lior Wolf. Unsupervised cross-domain image generation. *arXiv preprint arXiv:1611.02200*, 2016. 2, 4

[60] Yonglong Tian, Dilip Krishnan, and Phillip Isola. Contrastive multiview coding. *arXiv preprint arXiv:1906.05849*, 2019. 2

[61] Tongzhou Wang and Phillip Isola. Understanding contrastive representation learning through alignment and uniformity on the hypersphere. In *International Conference on Machine Learning*, pages 9929–9939. PMLR, 2020. 2

[62] Weiyue Wang and Ulrich Neumann. Depth-aware cnn for rgb-d segmentation. In *Proceedings of the European Conference on Computer Vision (ECCV)*, pages 135–150, 2018. 3

[63] Zhengwei Wang, Qi She, and Tomas E Ward. Generative adversarial networks in computer vision: A survey and taxonomy. *arXiv preprint arXiv:1906.01529*, 2019. 2

[64] Bichen Wu, Xuanyu Zhou, Sicheng Zhao, Xiangyu Yue, and Kurt Keutzer. Squeezesegv2: Improved model structure and unsupervised domain adaptation for road-object segmentation from a lidar point cloud. In *2019 International Conference on Robotics and Automation (ICRA)*, pages 4376–4382. IEEE, 2019. 3

[65] Shi Yan, Changlei Wu, Lizhen Wang, Feng Xu, Liang An, Kaiwen Guo, and Yebin Liu. Ddrnet: Depth map denoising and refinement for consumer depth cameras using cascaded cnns. In *Proceedings of the European conference on computer vision (ECCV)*, pages 151–167, 2018. 3

[66] Guandao Yang, Xun Huang, Zekun Hao, Ming-Yu Liu, Serge Belongie, and Bharath Hariharan. Pointflow: 3d point cloud generation with continuous normalizing flows. In *Proceedings of the IEEE/CVF International Conference on Computer Vision*, pages 4541–4550, 2019. 3

[67] Yaoqing Yang, Chen Feng, Yiru Shen, and Dong Tian. Foldingnet: Point cloud auto-encoder via deep grid deformation. In *Proceedings of the IEEE Conference on Computer Vision and Pattern Recognition*, pages 206–215, 2018. 3

[68] Yanchao Yang, Dong Lao, Ganesh Sundaramoorthi, and Stefano Soatto. Phase consistent ecological domain adaptation. In *Proceedings of the IEEE/CVF Conference on Computer Vision and Pattern Recognition*, pages 9011–9020, 2020. 2

[69] Yanchao Yang and Stefano Soatto. Fda: Fourier domain adaptation for semantic segmentation. In *Proceedings of the IEEE/CVF Conference on Computer Vision and Pattern Recognition*, pages 4085–4095, 2020. 2

[70] Li Yi, Boqing Gong, and Thomas Funkhouser. Complete & label: A domain adaptation approach to semantic segmentation of lidar point clouds. *arXiv preprint arXiv:2007.08488*, 2020. 3

[71] Zili Yi, Hao Zhang, Ping Tan, and Minglun Gong. Dualgan: Unsupervised dual learning for image-to-image translation. In *Proceedings of the IEEE International Conference on Computer Vision (ICCV)*, Oct 2017. 2

[72] Xiangyu Yue, Bichen Wu, Sanjit A Seshia, Kurt Keutzer, and Alberto L Sangiovanni-Vincentelli. A lidar point cloud generator: from a virtual world to autonomous driving. In *Proceedings of the 2018 ACM on International Conference on Multimedia Retrieval*, pages 458–464, 2018. 3

[73] Jin Zeng, Yanfeng Tong, Yunmu Huang, Qiong Yan, Wenxiu Sun, Jing Chen, and Yongtian Wang. Deep surface normal estimation with hierarchical rgb-d fusion. In *Proceedings of the IEEE/CVF Conference on Computer Vision and Pattern Recognition*, pages 6153–6162, 2019. 3

[74] Zhenyu Zhang, Zhen Cui, Chunyan Xu, Zequn Jie, Xiang Li, and Jian Yang. Joint task-recursive learning for semantic segmentation and depth estimation. In *Proceedings of the European Conference on Computer Vision (ECCV)*, pages 235–251, 2018. 3

[75] Sicheng Zhao, Yezhen Wang, Bo Li, Bichen Wu, Yang Gao, Pengfei Xu, Trevor Darrell, and Kurt Keutzer. epointda:

An end-to-end simulation-to-real domain adaptation framework for lidar point cloud segmentation. *arXiv preprint arXiv:2009.03456*, 2020. 3

[76] Chuanxia Zheng, Tat-Jen Cham, and Jianfei Cai. T2net: Synthetic-to-realistic translation for solving single-image depth estimation tasks. In *Proceedings of the European Conference on Computer Vision (ECCV)*, September 2018. 2

[77] Jun-Yan Zhu, Taesung Park, Phillip Isola, and Alexei A Efros. Unpaired image-to-image translation using cycle-consistent adversarial networks. In *Proceedings of the IEEE international conference on computer vision*, pages 2223–2232, 2017. 2, 4, 5, 6, 7, 8